Stability and secondary resonances in the spatial restricted three-body problem for small mass ratios

R. Schwarz[1]*, Á. Bazsó[1], B. Érdi[2], and B. Funk[1]

[1]*Institute for Astronomy, University of Vienna, A-1180 Vienna, Türkenschanzstrasse 17, Austria*
[2]*Department of Astronomy, Eötvös University, H-1117 Budapest, Pázmány Péter sétány 1/A, Hungary*

ABSTRACT

This paper is devoted to the study of secondary resonances and the stability of the Lagrangian point L_4 in the spatial restricted three-body problem for moderate mass ratios μ, meaning that $\mu \leqslant 0.0045$. However, we concentrated our investigations on small mass ratios $\mu \leqslant 0.001$, which represent the mass ratios for stable configurations of tadpole orbits in the Solar system.

The stability is investigated by numerical methods, computing stability maps in different parameter planes. We started investigating the mass of the secondary; from Earth-mass bodies up to Jupiter-mass bodies. In addition we changed the orbital elements (eccentricity and inclination) of the secondary and Trojan body. For this parameter space we found high order secondary resonances, which are present for various inclinations. To determine secondary resonances we used Rabe's equation and the frequency analysis. In addition we investigated the stability in and around these secondary resonances.

Key words: celestial mechanics – minor planets, asteroids – Solar system: general – methods: numerical

1 INTRODUCTION

Trojan asteroids are minor planets librating in the vicinity of the L_4 or L_5 points of a planet; e.g. Jupiter. L_4 and L_5 are equilibrium points and can be regarded as realizations of the Lagrangian triangular solutions of the restricted three-body problem which are stable for the mass ratio $\mu \lesssim 0.0385$, where μ is defined as $\mu = m_2/(m_1 + m_2)$; m_1 and m_2 are the masses of the primary and secondary bodies. The first Trojan asteroids were found in a 1:1 mean motion resonance with Jupiter, librating around the points L_4 or L_5 of the Sun-Jupiter system; preceding (L_4) or following (L_5) Jupiter at about 60°. Today we know approximately 6000 Trojans. Most of them are Jupiter Trojans (5984) but also one Earth Trojan, 4 Martian Trojans, one Uranus Trojan and 9 Neptune Trojans were detected (April 2014).

Several authors have conducted dynamical studies for Trojan asteroids in the Solar system (e.g. Robutel, Gabern & Jorba 2005; Marzari & Scholl 2013; Dvorak et al. 2007; Freistetter 2006; Érdi et al., Forgács-Dajka & Süli 2013) and the capture of Trojan asteroids Schwarz & Dvorak (2012). Robutel, Gabern & Jorba (2005) also investigated the secondary and secular resonances of Jupiter's Trojans by means of frequency map analysis. Some of these studies were dedicated to high inclined Trojan orbits (e.g. for Jupiter Trojans Schwarz, Gyergyovits & Dvorak (2004) and Dvorak & Schwarz (2005), for Neptune Trojans

Zhou, Dvorak & Sun (2009) and for Uranus Trojans Dvorak et al. (2010)). Érdi (1984) studied the critical inclination i_c of Trojan asteroids analytically. In a more general work of Brasser, Heggie & Mikkola (2004) they derived a formula[1] for the critical inclination as a function of the mass of the secondary body (planet):

$$i_c \approx 61.5°(1 - 1.123\mu). \tag{1}$$

Later investigations on high inclined orbits like by Funk et al. (2012) could confirm the results on i_c. In addition they found stable orbits (of the Trojans and the gas giant) for eccentricities up to 0.6 and for two different mass ratios $\mu = 0.001$ and $\mu = 0.007$. Close to these stability limits the Kozai resonance appeared, which is shown in the work of Zhou, Dvorak & Sun (2009) and Funk et al. (2012).

An interesting topic is also the possibility of Trojan planets in extrasolar planetary systems like it is discussed e.g. in the dynamical investigations of Nauenberg (2002), Érdi & Sándor (2005), Dvorak et al. (2004), and Schwarz et al. (2007).

In our Solar system, the eccentricities and inclinations of Trojan asteroids range widely and are often far greater than that of their host planet. This is discussed in the work of Schwarz, Funk & Bazsó (2013), where the stability was investigated for Trojan asteroids.

In continuation of our former work (Schwarz, Funk & Bazsó 2013) we concentrated our stability investigations now on lower

---

* E-mail:schwarz@astro.univie.ac.at

[1] The dependence on mass is rather weak for planetary size bodies

mass ratios $\mu \leqslant 0.001$. Therefore we investigated the stability of the Lagrangian point L_4 in the spatial restricted three-body problem to determine the stability limits for different masses of the secondary body. In addition we considered secondary resonances and their influence on the stability.

2   MODELS AND METHODS

We studied the spatial restricted three-body problem (SR3BP). In this problem two finite bodies, the primaries, revolve about their common centre of mass, and a third massless body moves under their gravitational influence not confined to the orbital plane of the primaries. We used the SR3BP in its variants: circular or elliptic spatial restricted three-body problem (C-SR3BP or E-SR3BP) depending on the orbit of the primaries. To study the stability in the equilibrium point L_4, for both cases – in the C-SR3BP and E-SR3BP – we integrated the equations of motion for the stability maps up to $T_c = 10^6$ periods of the primaries by using a Bulirsch-Stoer integrator and the Lie integration method complementary. For the boundaries between stable and chaotic regions or sticky orbits we integrated up to $T_c = 10^8$ periods. We also made long term calculations for a sample of resonant and non resonant orbits.

For the stability analysis we used the method of the maximum eccentricity e_{max} and the Lyapunov characteristic indicators (LCI). The results of the LCI and e_{max} are in a good agreement as shown in Schwarz et al. (2007); Schwarz, Süli & Dvorak (2009). The LCI is the finite time approximation of the maximal Lyapunov exponent. For the maximum eccentricity e_{max} we checked the largest eccentricity of the test particle during its motion. For larger eccentricities it is more probable that the orbit of the test particle becomes chaotic (having close encounters or even collisions with the primaries).

In order to obtain stability maps in the circular case, depending on the mass parameter μ of the primaries[2] and the orbital inclination i of the test particle, we changed the mass parameter μ between $1 \leqslant m_{Earth} \leqslant 1400$ (1400 Earth-masses is equal 4.5 Jupiter-masses) with a stepsize $\Delta m_{Earth} = 2$, and the initial inclination i between $0° \leqslant i \leqslant 60°$ with a stepsize $\Delta i = 10°$. In the elliptic case (E-R3BP), we changed μ in the same way, i between $0° \leqslant i \leqslant 60°$ with a stepsize $\Delta i = 10°$, and the orbital eccentricity e of the primaries between $0 \leqslant e \leqslant 0.99$ with a stepsize $\Delta e = 0.01$. Please note that the initial eccentricity of the test particle was always set to that of the secondary and we set $\varpi = 60°$ and $M = 0$.

As a consequence the test particle always started in L_4. The stability maps show either e_{max} or LCI for each orbit corresponding to the above mentioned initial conditions.

The classification of the orbit was done by checking the libration amplitude σ which is defined as the difference between the mean longitude of the asteroid and the planet ($\lambda_{Tro} - \lambda_P$). λ_{Tro}, λ_P are given by $\lambda_{Tro} = \varpi + M$, $\lambda_P = \varpi_P + M_P$ where ϖ, ϖ_P are the longitudes of pericenter of the massless body and of the planet and M_{Tro}, M_P are the mean anomaly of the third body respectively of the planet. This was already used in the work of Schwarz, Funk & Bazsó (2013). The difference to our former study is that we fix the initial eccentricity of the Trojan to that of the secondary body.

Another important point in this work is the analysis of the frequencies of the librational motion to determine secondary resonances. In a more general study of resonances Robutel, Gabern & Jorba (2005) did this for the Jupiter-Saturn system (fixed mass ratio). We computed also the frequencies of librational motions around L_4 and determined secondary resonances. In the planar, circular restricted three-body problem there are two frequencies, n_s and n_l, corresponding to the short and long period components of libration. In the planar, elliptic restricted three-body problem L_4 moves in an elliptic orbit itself and its mean motion n combines with n_s and n_l. Therefore, in the elliptic case there are four frequencies of libration n_s, n_l, $n - n_l$, and $n - n_s$. Rabe (1970, 1973) gave the normalized frequencies n_s and n_l taking n as unit frequency. Érdi et al. (2007, 2009) studied secondary resonances between the four frequencies and introduced several types. Type A corresponds to $(1 - n_l) : n_l$, type B to $n_s : n_l$.

To compute the frequencies of libration in the spatial case we used the Laplace-Lagrange variables h, k, p, q and the angle of libration σ given by

- $h = e \sin(\omega + \Omega), k = e \cos(\omega + \Omega)$

- $p = \sin i \sin \Omega, q = \sin i \cos \Omega,$

- $\sigma = \cos(\lambda - \lambda'), \lambda = \omega + \Omega + M.$

Here e is the eccentricity, i the inclination, ω the argument of pericentre, Ω the ascending node, λ the mean orbital longitude of the orbit of the test particle, and λ' is the mean orbital longitude of the smaller primary. (The angular orbital elements refer to the orbital plane of the primaries as reference plane, in which the reference direction points to the pericentre of the relative orbit of the primaries.)

Placing the test particle in L_4 with initial parameters described earlier, we followed its orbit for 10^6 periods of the primaries by using the Lie integrator and computed the corresponding h, k, p, q and σ variables to which we applied a discrete Fourier transform (DFT, with SigSpec), or a fast Fourier transform (FFT, via FFTW) to find the peaks in the power spectrum. The locations of the maxima are interpolated via a quadratic function, taking into account the three highest samples around the tentative peak. SigSpec computes the spectral significance levels for the DFT amplitude spectrum of a time series at arbitrarily given sampling. It solves for the probability density function of an amplitude level, including dependencies on frequency and phase (Reegen 2007). Frequency map analysis was used to investigate the stability properties of tadpole orbits in the proximity of the equilibrium points of Jupiter in the work of Marzari, Tricarico & Scholl (2003) and Robutel, Gabern & Jorba (2005).

3   STABILITY

In this chapter we concentrate our studies on the stability of the Lagrangian point L_4 in the spatial restricted three-body problem, for moderate mass ratios μ, meaning that $\mu \leqslant 0.0045$, which represents the mass parameter of up to 1400 Earth-masses (M_E) equal to 4.5 Jupiter-masses in the Solar system. The LCI stability maps are given in Fig. 1 for different inclinations ($i = 0, 10, 20, 30, 40, 50°$), starting with the planar case (Fig. 1 upper left graph). The graphs of Fig. 1 for higher inclinations show a structure that shift to smaller eccentricities. We could allocate the structure as the A 1:1 resonance. For comparison we included the well known analytical

---

[2] We decided to use the common definition of the dimensionless mass ratio μ as given in the introduction, and the dimensional mass parameter given in Earth-masses to compare more easily with the solar system

Table 1. The percentage of the number n of stable orbits for each stability map derived from Fig.1.

inclination [°]	n of stable orbits [%]
0	93
10	92
20	89
30	86
40	84
50	83
60	19

Table 2. The maximum eccentricity of test objects moving in stable tadpole orbits ($\sigma << 180°$).

inclination [°]	maximum eccentricity
0	0.77
10	0.73
20	0.69
30	0.64
40	0.62
50	0.61
60	0.02

curve of the A 1:1 resonance (Érdi et al. 2007) for the initial inclinations $i = 0, 10, 20°$ (Fig. 1 upper graphs and middle left graph) of the Trojan bodies. The curve (circles in black and white) fits well for $i = 0, 10°$, but does not fit anymore for $i = 20°$ and higher inclinations. This is because of the larger chaotic regions, which can be seen in Fig. 1, middle and lower graphs ($i = 20 - 50°$); $i = 60°$ is not presented, because there are only a few stable orbits.

For the conclusion we counted the number n (in percent) of stable orbits.

The results are presented in Tab. 1 for the different stability maps for different initial inclinations ($i = 0° - 60°$). We can conclude that the number of stable orbits for inclinations between $i = 0°$ and $i = 50°$ is almost constant and shrinks rapidly for $i = 60°$. The number of stable orbits can be given as the function of the inclination by a semi-empirical formula: $n = -0.22i + 93$. In addition we studied the variation of e_{max}. The stability maps gave the same results, therefore they are not shown here.

In addition we analysed the libration amplitude, because in the case of a large libration amplitude the Trojan may get on a horseshoe orbit or may be ejected out of the Trojan region after a close approach with the planet (secondary body). The value of σ should be smaller than $180°$ for tadpole orbits. Former studies (see Schwarz, Funk & Bazsó 2013) showed – by the help of the libration amplitude σ – that not all stable asteroids are moving in Trojan motion (= tadpole orbits). Therefore we checked the planar case and made a cut of our stability map shown Fig. 1 (upper left graph) in 0.001 (1 Jupiter mass) and 0.000117 (40 Earth masses) for 10^8 years. In addition we checked the libration amplitude for different inclinations for $\mu = 0.001$ shown in Tab. 2. We verified that the critical angles – we also call it libration amplitude σ – are oscillating around $\lambda_{Tro} - \lambda_P = 60°$ with a very small amplitude $\sigma = 10^{-6}$, even for e=0.75 and $\mu = 0.001$ (shown in section A).

Table 3. Initial points of the resonant curves obtained from Rabes equation (Rabe 1973) for the planar circular case (Fig 2 upper left graph).

| Type	Resonance	Frequency	μ	comment
A	19:1	0.95000000	0.00036972	new
B	20:1	0.99875234	0.00036880	?
A	9:1	0.90000000	0.00147099	new
B	10:1	0.99503719	0.00145652	?
A	11:2	0.84615385	0.00344712	new
A	4:1	0.80000000	0.00575455	
A	3:1	0.75000000	0.00883461	
A	1:1	0.50000000	0.02943725	Fig. 1

4 SECONDARY RESONANCES

Complementary to the stability analysis we made a frequency analysis to find new secondary resonances. Again we studied the stability maps depending on the orbital eccentricity e of the primaries and the mass ratio μ of the primaries. We placed the test particle in L_4 and started it on inclined orbits. Changing e and μ as described in Section 2, we followed the orbits for only 10 periods of the primaries and computed stability maps in the μ-e plane by recording the e_{max} and LCI values for each (μ, e) pair.

We studied the stability maps for a very short time (T_c=10 periods), because the structure of the secondary resonances are blurred for longer integration time. The stability maps are presented in Fig. 2 for $i = 0, 10, 20°$ (upper, middle and lower graph) and Fig. 3 present $i = 30, 40, 50°$, where the curves (lines) represent three different secondary resonances.

In case of $i = 0°$ (upper graph of Fig. 2) we show the analytical curves obtained from Rabe's equation (Rabe 1970, 1973), and in case of higher inclination we present the numerical results (by using frequency analysis). Obviously the curves obtained from Rabe's equation are not valid for higher eccentricities, but they are also valid for moderate eccentricities as was shown in Érdi et al. (2007). We could also find a shift of the resonances when we studied the spatial case for large μ (Schwarz et al. 2012). Were in Fig. 2 and Fig. 3 the results are shown for small μ. Before we go into the details we have to mention that the secondary resonances for small mass parameters are very close together and therefore not easy to locate. However, we found three new resonances – the A 19:1, A 9:1 and A 11:2 – which are shown for the planar case the upper left graph of Fig. 2 and the initial points are presented in Tab. 3. We note that the B 10:1 and the B 20:1 are also very close to the curve of A 19:1, but at the current resolution $\Delta\mu = 2M_E$ they are not distinguishable, because of the minimum distance of the resonances which is $\approx 0.5M_E$. However, the structures in the LCI seem to be associated preferably with the A-type resonances. These structures are visible in Figs. 2,3 but not labeled, because they are very close.

In addition we could allocate the A 4:1 (curve has an initial point at $e \approx 0.3$) and the A 3:1 resonances (curve has an initial point at $e \approx 0.4$). The last two resonances are not labeled in Figs. 2,3 and the initial points lie outside the scale of the graphs, because of their large mass ratio as shown in Tab. 3.

As mentioned before, the secondary resonances shift to higher mass parameter when the inclination increases. This can be seen clearly when we look at the initial points of the resonances ($e = 0$). The resonance A 19:1 for the planar case at 160 M_E is shifted to 200 M_E ($i = 50°$) see Fig. 2, which is a difference of $\Delta\mu = 40M_E$. The initial resonant point of the resonant curve A 9:1 is shifted from 490 M_E to 720 M_E ($\Delta\mu = 230M_E$) and for A 11:2 we
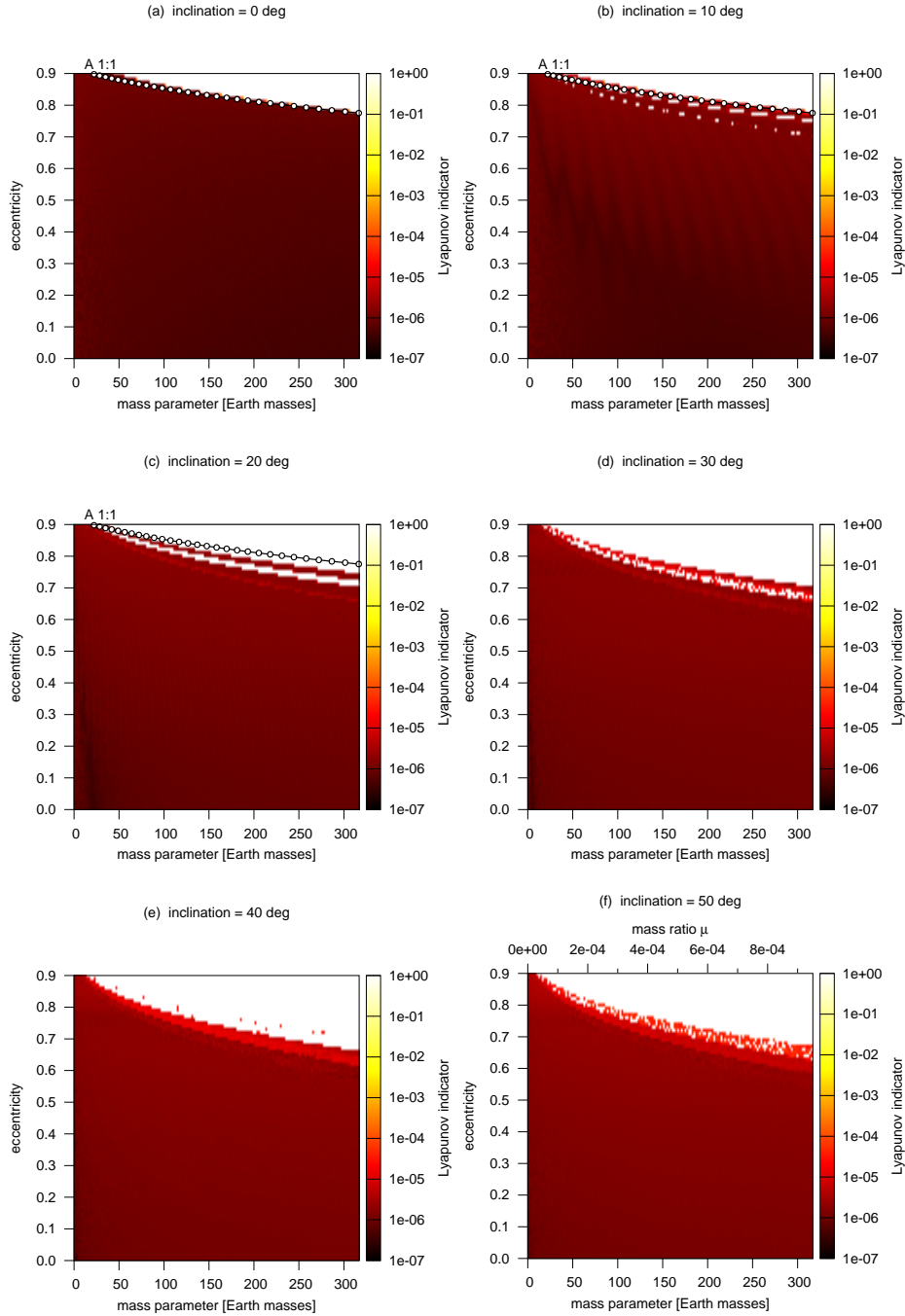
Figure 1. The LCI maps showing the stability of L_4 in the E-SR3BP depending on the eccentricity e and the mass parameter μ given in Earth masses, and for comparisons as mass ratio as defined in chapter1 (lower right graph). The dark red color depicts stable motion, whereas the yellow and white colors represent the chaotic behaviour. For color plots see online version. The circles in black and white represent the analytical curve of the A 1:1 resonance (given in the upper graphs and the middle left one).

measure a shift from 1150 M_E to 1700 M_E (lower graph Fig. 3) with a difference $\Delta\mu = 550M_E$. However, the shift with larger inclinations depend on the starting position of the resonance. That means that for low mass parameters the shift is smaller (A 19:1, $\Delta\mu = 40M_E$), whereas for larger values of μ the shift is larger (A 11:2, $\Delta\mu = 550M_E$).

Finally, we studied the long term stability of the resonances. For this we integrated orbits in, close to, and outside the secondary

resonances for a moderate initial eccentricity ($e = 0.2$, shown in Fig. 4) and a larger value of $e = 0.6$. An example is presented in Fig. 4, where we plotted the curve of the LCI for the complete integration time $T_c = 10^8$ periods, for 4 different orbits around the A 19:1 resonance. We can summarize that there is no difference in and outside the resonance and have no influence on the stability, but we have to remark that these are high order resonances. However,

this result show that the investigated secondary resonances will not play a role in the Solar system.

5 CONCLUSIONS

In this paper we studied the stability of the Lagrangian point L_4 in the spatial restricted three-body problem (SR3BP). It is known that in the planar, circular restricted three-body problem L_4 is linearly stable for mass ratios $\mu \lesssim 0.0385$. However, we concentrated our investigations on small mass ratios $\mu \leqslant 0.001$, which represents the mass ratios for stable configurations of tadpole orbits in the Solar system. We computed different stability maps in the SR3BP by changing the orbital inclination ($\Delta i = 10°$) of the test particles. However, the stability maps were computed by changing the mass parameter and the eccentricity of the primaries; for a very fine grid of initial conditions ($\Delta\mu = 2M_E$ and $\Delta e = 0.01$).

The stability analysis had shown that the size of the stable region of the stability maps (μ-e plane) shrinks with the increase of the inclination (Fig.1). The decrease of the number of stable orbits (in percent of all orbits) is almost linear with respect to the increase of the inclination and dropping down abruptly at $i = 50°$; shown in Tab.1. We could confirm – by computing the libration amplitude – our former results that the stability maps mainly show tadpole orbits. The small libration amplitude follows from the initial conditions starting in the equilibrium point L_4 with equal eccentricity of the secondary and Trojan body.

Our investigations showed that there exist also secondary resonances for small μ. Using Rabe's equation (Rabe 1973) and frequency analysis we could determine the A-type 19:1, A 9:1 and the A 11:2, which are high order resonances. We found also B-type resonances, but at the current resolution they are not distinguishable from the A-type resonances. We can conclude that these resonances have no influence on the orbital stability (Fig. 4). Nevertheless we could show that the secondary resonance A 1:1 is relevant for the stability and shifts with larger inclinations. We could also show that a few resonances whose initial points lie in the region of higher mass ratio (presented in Érdi et al. (2007)) move into the region of low mass ratios. Also the well known analytical curve of the A 1:1 resonance move into the region of low mass parameter. For initial inclinations $i = 0°, 10°$ (Fig. 1 upper graphs and middle left graph) the curve fits well with the limit between stable and unstable region, but it does not fit anymore for $i = 20°$ and higher inclinations (the different types of resonances were defined in Érdi et al. (2007) for the planar case), because the A 1:1 resonance shifts to lower eccentricities.

Further investigations have to be done to investigate the long term stability of the secondary resonances and to find new ones.

REFERENCES

Brasser, R., Heggie, D., Mikkola, S., 2004, CeMDA, 88, 123
Dvorak R., Pilat-Lohinger E., Schwarz R., Freistetter F., 2004, A&A, 426, L37
Dvorak R., & Schwarz R., 2005, CeMDA, 92, 19
Dvorak R., Schwarz R., Süli Á. Kotoulas, T., 2007, MNRAS, 382, 1324
Dvorak R., Bazsó Á., Zhou L.-Y., 2010, CeMDA, 107, 51
Érdi, B., 1984, CeMDA, 34, 435
Érdi B., Sándor Zs., 2005, CeMDA, 92, 113
Érdi B., Nagy I., Sándor Zs., Süli Á., Fröhlich G., 2007, MNRAS, 381, 33
Érdi B., Forgács-Dajka E., Nagy I., Rajnai R., 2009, CeMDA, 104, 145
Érdi B., Forgács-Dajka E., Süli Á., 2013, CeMDA, 117, 3.
Freistetter F., 2006, A&A, 453, 353
Funk B., Schwarz R., Süli Á., Érdi B., 2012, MNRAS, 423, 3074-3082
Marzari F., Tricarico P., Scholl H., 2003, MNRAS, 345, 1091.
Marzari F., Scholl H., 2013, CeMDA, 117, 91.
Nauenberg M., 2002, AJ, 124, 2332
Rabe E., 1970, in Giacaglia G.E.O., ed., Periodic Orbits, Stability and Resonances. D. Reidel Publ. Co., Dordrecht, p. 33
Rabe E., 1973, in Tapley E.D., Szebehely V., eds, Recent Advances in Dynamical Astronomy. D. Reidel Publ. Co., Dordrecht, p. 156
Reegen P., 2007, A&A, 467, 1353
Robutel P., Gabern F., Jorba A., The observed Trojans and the global dynamics around the Lagrangian points of the Sun Jupiter System, CeMDA, 92, 53 (2005)
Schwarz R., Gyergyovits M., Dvorak R., 2004, CeMDA, 90, 139
Schwarz R., Dvorak R., Süli Á. and Érdi B., 2007, A&A, 474, 1023
Schwarz R., Süli Á., Dvorak R., 2009, MNRAS, 398, 2085
Schwarz R., Dvorak R., 2012, CeMDA, 113, 23
Schwarz R., Bazsó Á., Érdi B., Funk B., 2012, MNRAS, 427, 397
Schwarz R., Funk B., Bazsó Á., 2013, MNRAS, 436, 3663
Sicardy B., 2010, CeMDA, 107, 145
Zhou L-Y., Dvorak R., Sun Y-U., 2009, MNRAS, 398, 1217
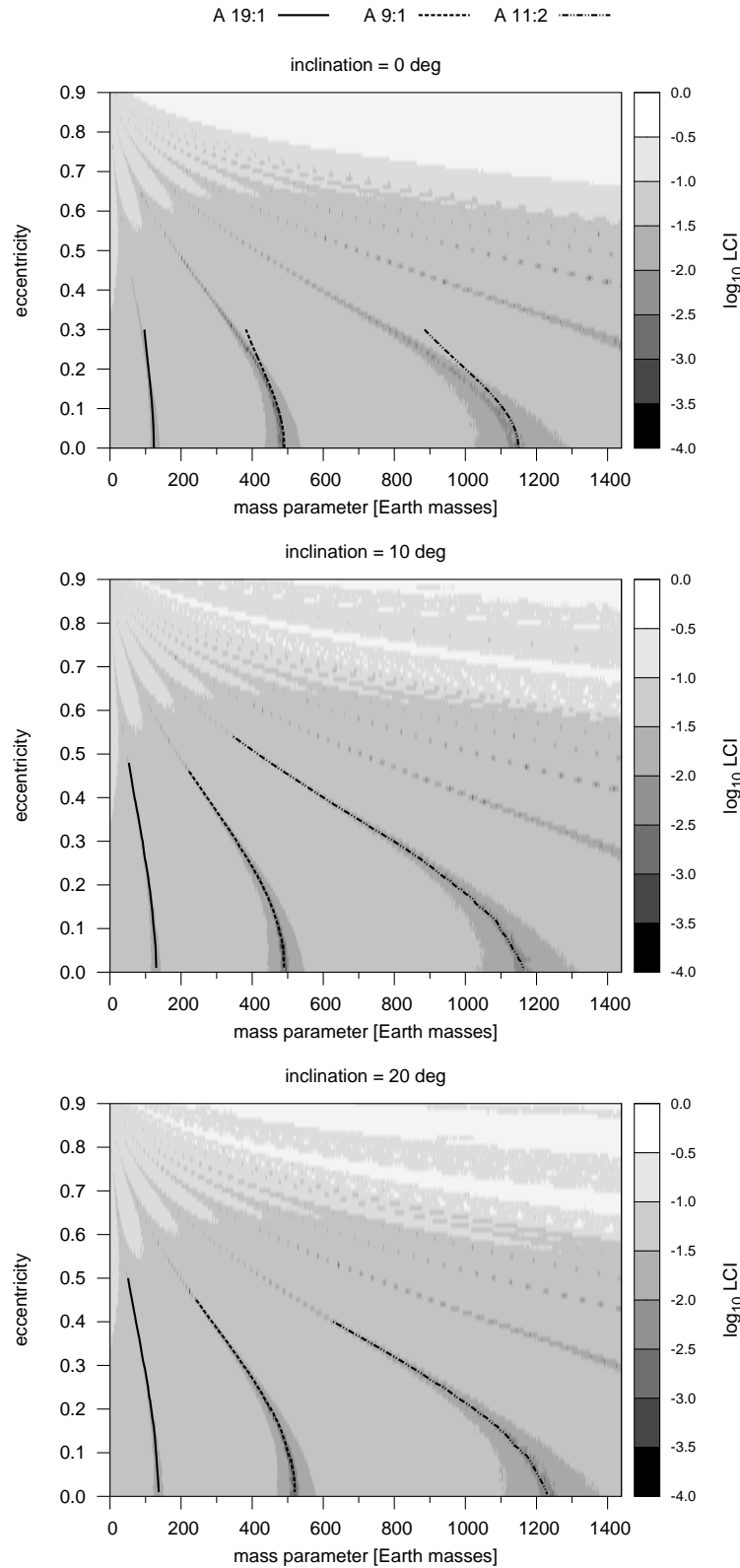
APPENDIX A: CRITICAL ARGUMENT

With Fig. A1 we checked the critical argument (maximum and minimum value) for a time spane up to 10^5 years. We found out that the critical argument shows small oscillations (about 10^{-6}). For the cases a) and b) we can see that the eccentricity is very constant, however for case c) where we move away from the Lagrangian point we observed chaotic behaviour within 20000 years. We have to remark that our investigations represent the case a).
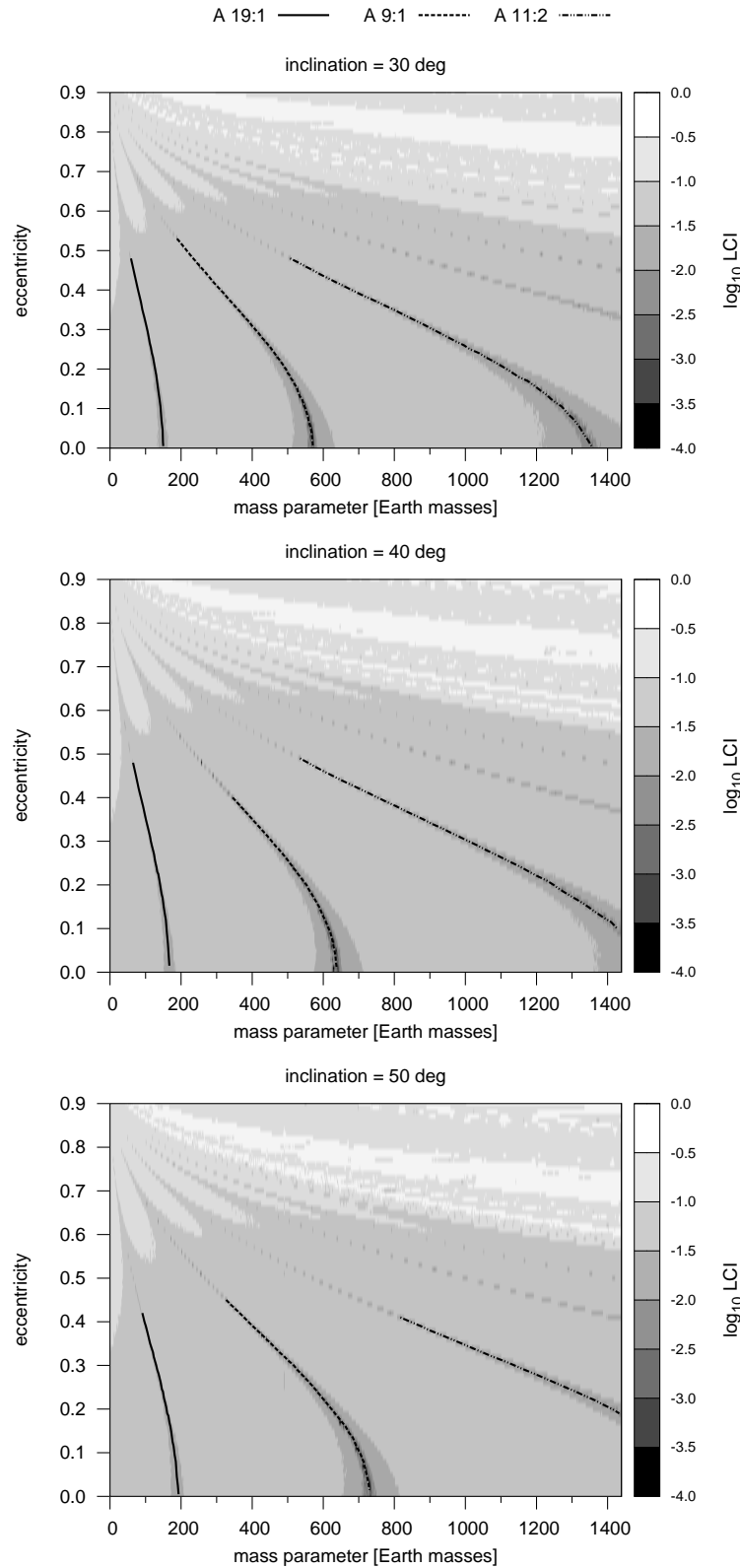
Figure 2. The LCI maps showing the stability of L_4 depending on the eccentricity e and the mass parameter μ. The dark grey region depicts stable motion, the light regions correspond to chaotic behaviour. The lines represents three different resonances; in case of $i = 0°$ (upper graph) the analytical curves were obtained from Rabe's equation (1970), whereas in case of $i = 10°$ (middle graph) and $i = 20°$ (lower graph) the curves presents the results of the frequency analysis.

A 19:1 ——— A 9:1 ---------- A 11:2 ·—·—·—·

inclination = 30 deg

inclination = 40 deg

inclination = 50 deg

Figure 3. The LCI maps showing the stability of L_4 depending on the eccentricity e and the mass parameter μ. The dark region depicts stable motion, the light regions correspond to chaotic behaviour. The curves represents three different resonances in case of $i = 30°$ (upper graph), $i = 40°$ (middle graph) and $i = 50°$ (lower graph) obtained by frequency analysis.
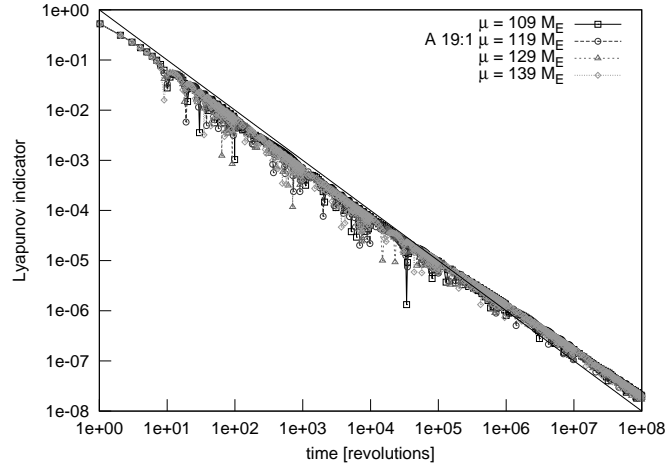
Figure 4. The LCI for $T_c = 10^8$ periods for 4 different orbits (different masses) in, close and out of the secondary resonance A 19:1. The diagonal line represents the theoretical behaviour of the Lyapunov exponent decreasing inversely proportional with time.
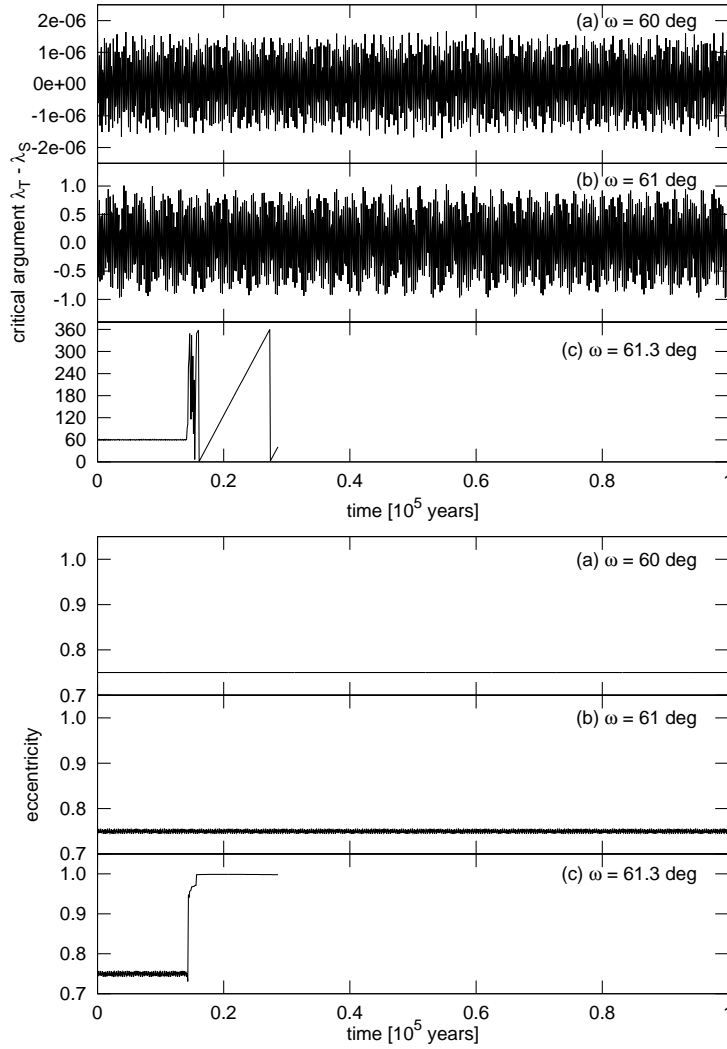
Figure A1. The critical argument for libration for a time span of 10^5 years and eccentricity e for the mass parameter $\mu = 0.001$. The three cases (a-c) show the different argument of perihelion ω, except that the initial e of the secondary and the Trojan body is the same.